REPORT DOCUMENTATION PAGE

Form Approved
OMB No. 0704-0188

PLEASE DO NOT RETURN YOUR FORM TO THE ABOVE ORGANIZATION.

1. REPORT DATE *(DD-MM-YYYY)*	2. REPORT TYPE	3. DATES COVERED *(From - To)*
02-05-2010	Final Technical Report	

4. TITLE AND SUBTITLE
Self-assembled Combinatorial Nanoarrays for Multiplex Biosensing

5a. CONTRACT NUMBER

5b. GRANT NUMBER
FA9550-07-1-0080

5c. PROGRAM ELEMENT NUMBER

6. AUTHOR(S)
Hao Yan

5d. PROJECT NUMBER

5e. TASK NUMBER

5f. WORK UNIT NUMBER

7. PERFORMING ORGANIZATION NAME(S) AND ADDRESS(ES)
Arizona State University

8. PERFORMING ORGANIZATION REPORT NUMBER

9. SPONSORING/MONITORING AGENCY NAME(S) AND ADDRESS(ES)
AFOSR/RSL
875 N Randolph St
Arlington, VA 22203

10. SPONSOR/MONITOR'S ACRONYM(S)

11. SPONSOR/MONITOR'S REPORT NUMBER(S)
AFRL-SR-AR-TR-10-0126

12. DISTRIBUTION/AVAILABILITY STATEMENT

DISTRIBUTION A: Approved for Public Release

13. SUPPLEMENTARY NOTES

20100426222

14. ABSTRACT

In 2009, we have studied multivalent DNA hybridization in a nanostructured system. We have used lithographically patterned substrate to direct the assembly of DNA nanoarrays. We have succeeded in in-vivo cloning of DNA nanostructures.

15. SUBJECT TERMS

16. SECURITY CLASSIFICATION OF:			17. LIMITATION OF ABSTRACT	18. NUMBER OF PAGES	19a. NAME OF RESPONSIBLE PERSON
a. REPORT	b. ABSTRACT	c. THIS PAGE			Hao Yan
					19b. TELEPHONE NUMBER *(Include area code)* 480-727-8570

Final Project report

FA9550-07-1-0080

Self-assembled Combinatorial Nanoarrays for Multiplex Biosensing

Principle Investigator: Hao Yan
Department of Chemistry and Biochemistry &
The Biodesign Institute
Arizona State University

Reporting period: 01/01/07-11/30/09

1. Project Goal: This AFOSR-YIP program aims to develop a new technology to construct ***self-assembled, water-soluble***, and ***combinatorial*** nanoarrays for multiplex detection of biological relevant molecules. This technology will open up new opportunities using combinatorial methods for a wide range of military and security applications ranging from sensor arrays for the detection of lethal viruses and tumor markers to information encryption devices.

2. Technical Accomplishments:

2.1 Self-assembled Combinatorial Encoding Nanoarrays for Multiplexed Biosensing

Multiplexed and sensitive detection of nucleic acids, proteins or other molecules from a single solution and a small amount of sample is of great demand in biomarker profiling and disease diagnostics. Here we describe a new concept using combinatorial self-assembly of DNA nano-tiles into micron-sized 2D arrays that carry nucleic acids probes and barcoded fluorescent dyes to realize multiplexed detection. We demonstrated the specificity and sensitivity of the arrays by detecting multiple DNA sequences and aptamer binding molecules. This DNA-tile array based sensor platform can be parallelly constructed through DNA oligonucleotides self-assembly. The attachment of different molecular probes can be achieved by simple DNA hybridization so no bio-conjugation is necessary for the labeling. Accurate control of the inter-probe distances and solution based binding reactions ensures fast target binding kinetics.

Barcodes are a part of our everyday life for tracking information. Similarly, if each individual biological recognition event can be encoded by a specific barcode that can be easily read out, one can build a multiplexed sensing system for a large number of molecular species from a single solution with a small amount of sample. The current multiplexing detection methods for nucleic acids and proteins utilize either chip-based platforms or particle-based platforms. For the chip based detection, a large number of different probes for proteins or nucleic acids are immobilized on a planer solid support that the identities of the probes are labeled as a specific positional address on the planar array. While for the bead-based detection, the different probes are conjugated on the surface of micron-sized particles, that each has a specific spectral fingerprint to reveal the identity of the probes that it carries. Recently, Luo and co-workers demonstrated that dendrimer-like DNA can be constructed as nanobarcodes through enzymatic ligation for multiplexed detection of pathogens. Herein, we describe a new strategy of creating barcoded multiplexing detection system, which is based on the platform of a fast developing technology called DNA tile self-assembly.

The construction of synthetic nano-architectures based on DNA tile self-assembly has seen rapid progress in the past few years. DNA is an ideal structural material due to its innate ability to self-assemble into highly ordered structures with nanometer scale features based on the simple rules of Watson-Crick base pairing. DNA tile molecules can self-assemble into micro- to millimeter sized 2-dimensinal (2D) lattice domains made from millions to trillions of individual building blocks. A

unique advantage of these self-assembled DNA tile arrays is the ability to assemble molecular probes with precisely controlled distances and relatively fixed spatial orientations.

The idea of the self-assembled encoding arrays is illustrated in Figure 1a. Here we utilize a previously developed AB tile system of cross-shaped tile structures, but modified the A tiles with organic dyes for spectral encoding and B tiles with single stranded probes for detection. The sticky ends of the tiles are designed in a manner that the A tiles and B tiles separately do not associate with themselves, but when mixed, they can associate with each other alternatively to form 2D lattices, with a high reproducibility and yield. Two sub-groups of A tiles, A1 modified with a "red" dye (Cy5), and A2 modified with a "green" dye (Rhodamine Red-X), are used to perform the encoding. Each sub-set of B tiles carries a different detection probe that is labeled with a "blue" dye (Alexa Fluor 488). All B tiles share the same sticky ends, so that they can bind to A tiles to form the 2D lattice. The probes are not involved in the DNA tile array formation but dangling out of the array plane through base-paring with the anchor probes that are single stranded extensions of one of the strands within the DNA tile (schemed in Fig. 1b). Their sequences can be changed readily as desired for the different target binding purposes. Examples of probes on the B tiles include single stranded oligonucleotides for detection of DNA or RNA targets, or aptamers for specific aptamer binding molecules. Aptamers are short DNA or RNA sequences that, through an *in vitro* selection process, display high specificity and affinity to specific ligand molecules, such as proteins or small molecules. Similar to the single stranded nucleic acid probes, aptamers can be attached to the DNA tile array simply by a short stretch of DNA hybridization (Fig. 1b). With two encoding dyes, the capacity of the multiplex detection system is determined by the number of different intensity levels in the two encoding channels ("red" and "green") that can be distinguished by the fluorescence microscope detector.

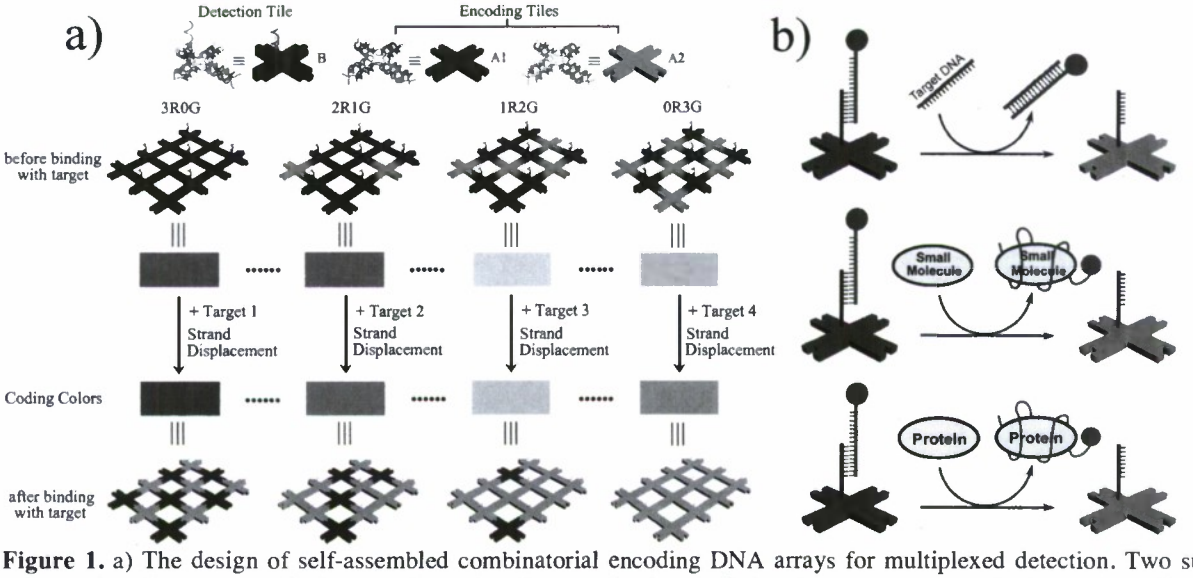

Figure 1. a) The design of self-assembled combinatorial encoding DNA arrays for multiplexed detection. Two sub-groups of A tiles, A1 modified with a "red" dye (Cy5), and A2 modified with a "green" dye (Rhodamine Red-X), are used to perform the encoding. B tile each carries a detection probe that is labeled with a "blue" dye (Alexa Fluor 488) act as the detection tile. Each sub-groups of B tiles carries a different probe, but shares the same sticky ends, so that each subset of B tiles can bind to A tiles to form the 2D lattice. The probes are not involved in the DNA tile array formation but dangling out of the array plane through base-paring with the anchor probes that are single stranded extensions of one of the strands within the DNA tile. By mixing the A1 and A2 tile at different ratios and then mix A tile and a certain B tile at a (A1+A2):Bi = 1:1 ratio, a series of different colored detection arrays can be generated. b) The detection mechanism. A target binding with the probe displaces the dye-labeled probe (blue) causing a color change of the tile array from the blue-masked color to the two color-mixed encoding color as indicated by the arrows connecting the rectangles in the middle of a). This mechanism can detect nucleic acid oligos with their complementary DNA probes, and proteins or small molecules with their specific aptamers.

The assembly of the multiplex detection array includes the following steps: 1) A1 tile ("red" dye labeled) and A2 tile ("green" dye labeled) are annealed separately, and then mixed together at various molar ratios in different tubes to generate a combinatorial series of barcoded mixtures, e.g. 3R0G, 2R1G, 1R2G, and 0R3G; 2) Different probes all labeled by the same "blue" dye are annealed into B tiles in different tubes; 3) By mixing the barcoded mixtures of A tiles with the subsets of B tiles one to one correspondingly in separate tubes with a ratio of (A1+A2):B = 1:1, the A tiles will associate with the B tiles to grow into 2D arrays. So that a modular system of encoding arrays is set up, with each array carrying a unique probe and displaying a unique barcode color (see examples in Fig. 2, left column); 4) All of the barcoded arrays are mixed together at room temperature to form the multiplexed detection system (see examples in Fig. 3a, with no target). The different array domains, each carrying a unique probe, will co-exist in a single solution. Thermodynamically, these arrays are prone to stick to each other as they share the same complementary sticky ends on the edges of the array, and indeed overlapping and touching edges of same and different colored arrays are sometimes observed in high concentration samples of the arrays. This does not interfere with the specificity of the detection. The micron-sized arrays each contains millions to billions strands of oligonucleotides, so that they have much lower diffusion rates compared to that of the individual oligonucleotides free in solution. At low concentrations, < 100 nM, without a thermal cycling procedure (raise the temperature then cooling down), the complementary sticky ends have very low chance to bind to each other, so they are more separated as observed under the microscope.

The mechanism of the detection is through a strand displacement (Fig. 1b). Addition of a target molecule will bind to its specific probe and displace the probe from the array. This occurs because the target binding to the probe initiates a branch migration between the probes and the anchor probes on the tile. This is "fueled" by the free energy released from the fully complementary base pairing between the DNA probe and its target DNA oligos, or a stronger binding between the aptamer and its specific target molecule. These strand displacements have been previously used to construct DNA based mechanical nanodevices[30-33] and to control binding and releasing of thrombin protein with its aptamer[34]. Here the target-probe complex is released from the array surface, leaving behind the empty anchor probe on the tile. This process leads to disappearance of the "blue" color on the tile array, so that the array changes color from the "blue-masked" color into the original encoding color from A tiles only. This color change can be observed by fluorescence microscope when the arrays are deposited on the surface of a slide. The identity of the target binding event on each array is coded by the specific color of the array (relative fluorescent intensity of the two encoding dyes). The color change however can not be observed by regular fluorometer in solution, because no separation of the detached probe strand from the mixture solution is carried out. But under fluorescence microscope, the signal intensity is counted as photon counts per pixel area with a pixel in the image ~ 200 nm in both x and y dimensions. The individual DNA strands have much less tendency to stay on the surface compared to the large DNA lattices, and even if they stay on the surface, they are adsorbed randomly and loosely, their contribute to the background signal, is much less than the signal from the densely and regularly packed probes on the arrays. For the 2D DNA arrays lying flat on the substrate, the signal level from different sized arrays are the same (in the red and green channels) as long as the array size is greater than the pixel size. This is because the dye labels on the array spatially evenly distributed on the 2D DNA lattice. The heterogeneous size distribution of the DNA arrays contribute little signal heterogenity in the detection. That is why the fluorescence microscopy is a better detection method in using the DNA arrays for sensing[24].

The self-assembled combinatorial encoding arrays described above are expected to possess the following unique features: 1) Parallel synthesis of custom arrays. A 100 nanomole-scale DNA synthesis yields $>10^{10}$ arrays (assuming in average ~10x10 μm^2 in dimension for each array). Different types of arrays can be made modularly with small changes to the component oligonucleotides, and the formation of the DNA arrays are by mixing the DNA oligos in the right ratios and it is completed solely by self-assembly in a slow cooling step; 2) No bio-conjugation steps are necessary to attach probes to the array. The detection mechanism is based on DNA or RNA strand hybridization and

displacement. Molecular capture probes (either DNA, RNA or aptamer oligos) are partially hybridized to the DNA tile in the array through hydrogen bonding of base pairs. No covalent bonding process is involved in this process. This significantly reduces steps in the detection system preparation, compared to the chip or bead-based technologies. For the same reason, the detection system is also rechargeable, because after each round of detection, additional molecular probes can be added to the solution of the array and rehybridized into the array for the reuse of the detection system; 3) Accurate control of spatial distance between probes and binding process in solution allow more efficient binding of targets to the probes: The rigidity and well-defined geometry of the DNA tile structures provide spatial and orientational control of the probes on the array. The spacing of the probes and their positioning with respect to the tile array surface can be precisely controlled to the sub-nanometer scale. As designed, the dimensions of all the tiles are ~ 19 nm across, and the distance between the centers of the two neighboring A tiles or B tiles is ~ 27 nm. Each tile carries only one probe sequence labeled with one dye molecule, which points out of the plane of the array. In the most extended form, the probe is no more than 10 nm long. The well-controlled spacing between the tiles prevents energy transfer processes such as self quenching or fluorescence resonance energy transfer between the neighboring dye molecules. This ensures accurate reading of the spectral codes. It also prevents interactions between the single stranded probes on the tile arrays, this not only allows optimization of geometry for fast kinetics due to low steric hindrance, it also allows efficient rebinding of the target to nearby probes and leads to improved binding efficiency. 4) Simultaneous detection of various biomolecular species. Aptamers have been selected to bind with a variety of molecules or species. They are compatible with the DNA based tile arrays and can be easily incorporated into the tile array and keep their activities for their specific binding properties. Different encoded tile arrays can each carry a unique aptamer sequence as probes, so that the presence of multiple aptamer binding species of vast different properties in a mixture can be detected simultaneously.

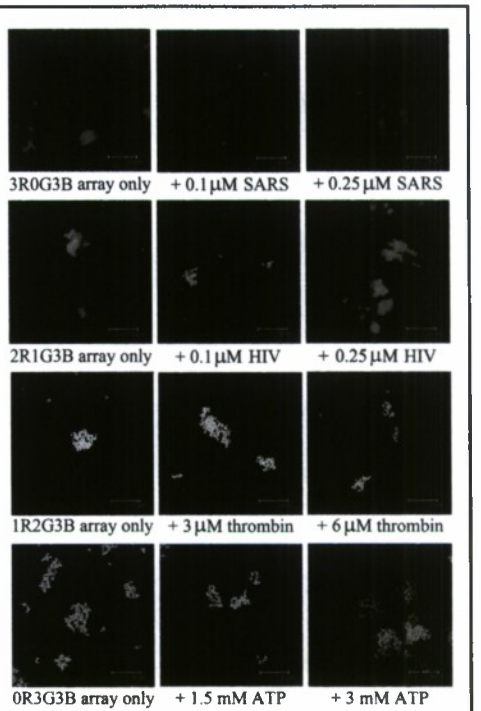

Figure 2. Titration of the targets against the encoding arrays. Four types of arrays are prepared separately, each (0.25 μM) carries a blue probe on B tile: 3R0G3B (probe1), 2R1G3B (probe2), 1R2G3B (probe3), 0R3G3B (probe4). The targets and concentrations used are listed below each image. Scale bar: 30 μm.

To demonstrate the function of the arrays, four types of color-encoded arrays are prepared separately, each carrying a blue probe on the B tile: 3R0G3B (probe1), 2R1G3B (probe2), 1R2G3B (probe3), and 0R3G3B (probe4). The four probes corresponding to the four targets: probe 1 and 2 are the complementary sequences of the two virus DNA sequences, severe acute respiratory syndrome virus (SARS) and the human immunodeficiency virus (HIV), probe 3 and 4 are the aptamer sequences that can specifically bind to Human α-thrombin and adenosine triphosphate (ATP), respectively. Titration experiments reveal the color changes upon addition of the specific targets separately in increasing concentrations to the corresponding encoded array (Fig. 2). As expected, the color of the arrays change from the "blue-masked" colors to the "green-red" encoded colors, with clear transitions between the partial binding and saturated binding of the probes.

We have tested the concept of combinatorial encoding by detecting multiple DNA targets simultaneously from a single solution (Fig. 3a). Four DNA targets are used, two are the partial sequences of the virus genome, and the other two are the complementary sequences of the two aptamers used (sequences of thrombin and ATP aptamers). The four types of color-encoded arrays are mixed together. Upon addition of the targets individually or in different combinations of mixtures, the

presence of each target reveals a color specific coded to the array containing the probe for that target. Target 1 displaces the blue color from 3R0G3B (pink) and reveals 3R0G (red). Similarly, target 2 reveals 2R1G (orange), target 3 reveals 1R2G (yellowish green), and target 4 reveals 0R3G (green). The specificity of the multiplex detection is indicated by the lack of color change of the arrays when their specific targets are absent (Fig. 3a). Probes of different lengths are used, ranging from 21 to 39 nucleotides. The number of base-pairing between the probes and the anchor strands on the tiles are also different, ranging from 8 to 12 base-pairs. The detection of targets of different lengths all display similar efficiency, showing versatility of the detection system.

We have used the encoding array for multiplexed detection of aptamer binding molecules (Fig. 3b). The existence of the targets, human α-thrombin (target 5) and ATP (target 6), individually or in a mixture, reveals their corresponding encoding color in the array (Fig. 3b). The arrays carrying probe 1 and probe 2 do not show any color change, demonstrating the probe specificity of the multiplexed detection. As a control experiment, the existence of 6 μM of bovine serum albumin (BSA) protein does not lead to the color change of all the encoding arrays (left panel, Fig. 3b), showing the target specificity of the detection.

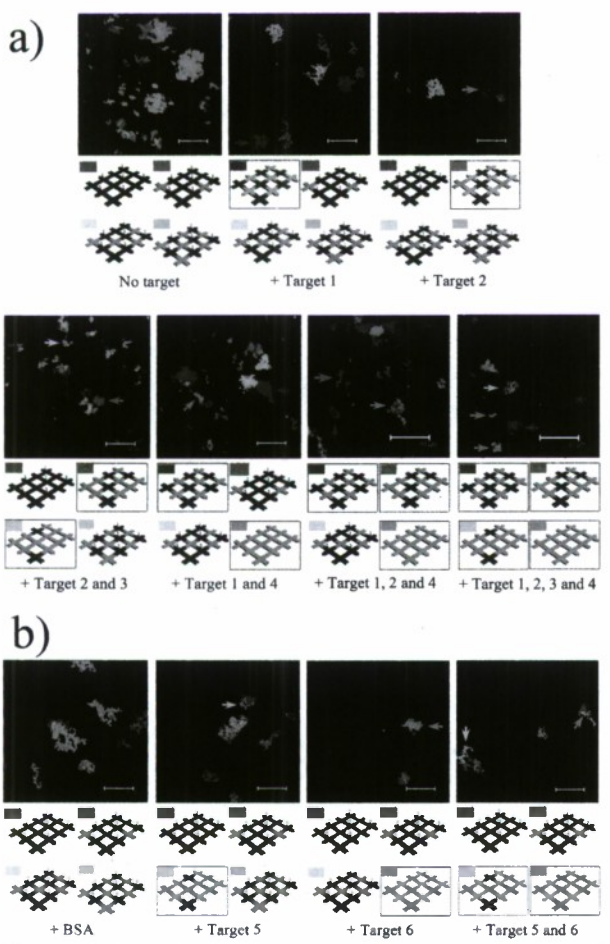

Figure 3. Combinatorial encoding array for multiplexed detection of DNA oligos, protein and a small molecule. Four types of arrays (same as in Figure 2) are mixed together. The combinations of targets added to the array are indicated as schematics below each image. The arrows point to the appearance of the encoding colors. Scale bars: 30 μm. a) Multiplexed detection of four different DNA targets. b) Multiplexed detection of two aptamer binding molecules.

To generalize the application of the detection system for real-world complex sample, we have performed the detection of DNA samples in bovine serum (Fig. 4). Note that in the present of only bovine serum, greenish yellow (1R2G) encoding color was revealed. This is because micro-molar concentration of thrombin exists in serum. SARS DNA (target 1), HIV DNA (target 2) and the complementary strand to ATP aptamer (target 4) can all be detected without any ambiguity. Target 3 is the complementary strand to the thrombin binding aptamer. Same color change is expected for the presence of target 3 or thrombin. Although there is also ATP in serum, the concentration was too low (~ 2 μM) to be detected by the current concentration of array, which detects ~ 1 mM ATP.

The detection limit is related to the effective probe concentration in the detection system and the dissociation constant of the target-probe complex. The apparent dissociation constants for the aptamer binding molecules are ~ 400 nM for thrombin and ~ 600 μM for ATP, much weaker binding affinities compared to the DNA/DNA duplexes with 12 bp (K_D in pM range). Thus, higher concentrations of these two aptamer targets are needed to get the similar amplitudes of color change in comparison to DNA/DNA duplexes target/probe binding. To further refine the detection sensitivity, we need to use lower concentration of the probes and to optimize the affinities between the probes with their aptamer targets.

We performed a test to detect lower amounts of the four DNA targets by diluting the arrays to 5 nM. The appearance of four different encoding colors after addition of 5 nM of each DNA targets indicated that it is possible to lower the detection limit by diluting the tile arrays. It is noted that the binding kinetics is fast as the color change of the fluorescence imaging signal was observed within 15-20 minutes after the addition of the target. This is a very quick detection compared to other methods mentioned in the introduction, which generally required hours of hybridization and hours of sample treatments after the target binding step. When performing detection by fluorescence microscopy, we spread out the sample (2.5 μL) to the whole surface area of an 18 mm square cover slip. In this case, we sometimes had to manipulate the sample stage to locate all the different arrays, which limited the throughput of the detection. The throughput of the detection can be improved by increasing the surface coverage of the DNA tile arrays on the sample slide, which can be achieved by confining the sample deposited on the surface to a sub-millimeter area, for example using a micro-arrayer to deposit ~ nano-liter of samples on the substrate, the spot sizes can be as small as 200 μm. If we are not limited by the throughput of the detection, sub-pM to fM detection sensitivity for DNA targets could be achieved. Detection mechanism using positive signal change schemes (in stead of the negative signal scheme used herein) can also be designed. When combined with signal amplification techniques, such as DNA hybridization chain reaction[43] on the encoding array, even higher sensitivity might be achieved. More efforts are carried out in this direction to optimize the detection sensitivity and throughput.

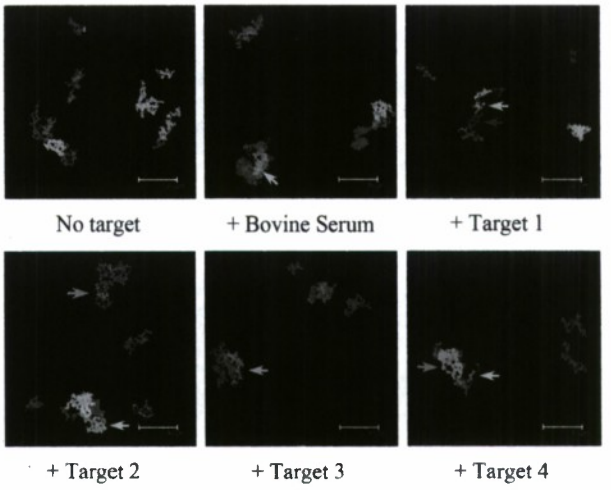

Figure 4. Combinatorial encoding array for detection of DNA oligos in bovine serum. Synthetic DNA oligo was spiked into 2 μL bovine serum (Sigma), in which DNase was pre-inhibited by aurintricarboxylic acid (ATA), before added into 10 μL mixture of array. Final concentration of DNA oligo target was 0.4 μM. The target added to the array is indicated below each image. The arrows point to the appearance of the encoding colors. Scale bars: 30 μm.

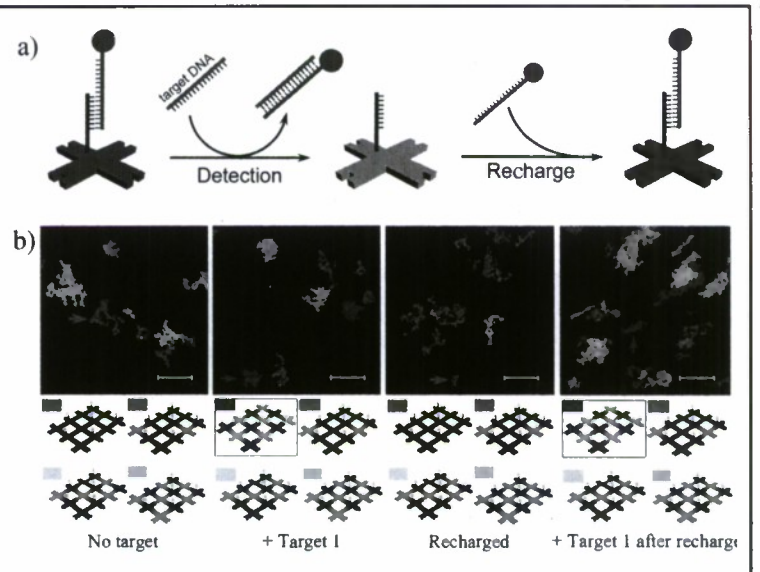

Figure 5. *The recharging of the encoding array for repeated use.* a) Schematic illustration of the recharging process. b) Experiments demonstrating the recharging. From left to right: mixture of the four encoded arrays with no target; after addition of target 1, the pink array turned red, revealing the detection; after addition of the probes for target 1, the color of the red arrays turned pink, returning to the original state; the recharged array mixture is capable to run another round of detection. The arrows point to the arrays with expected color change.

In summary, we have described a new strategy utilizing DNA tiles to direct the self-assembly of fluorescently labeled molecular probes into combinatorial encoding arrays for multiplexed detection. The simplicity, cost efficiency, high adaptability, quick detection are the most valuable and unique features that the new system provides. The technology

developed here could possibly be used widely in regular research lab or clinic labs routinely for small to moderate scale protein profiling and gene expression detection.

2.2 Recharging the combinatorial encoding array detection system

One of the original goals of the project is to develop the combinatorial encoding nanoarray system that can have recharging ability (reusability). We successfully demonstrated that the detection system is rechargeable. After each round of detection, additional molecular probes can be added to the solution of the array and rehybridized into the array for the reuse of the detection system. Figure 5 shows the recharging of the array.

2.3 Signal Amplification on a DNA Tile based Biosensor with Enhanced Sensitivity

Another goal in the project is to enhance the detection sensitivity for the combinatorial detection array system. This was achieved by utilizing hybridization chain reaction (HCR) as a signal amplifier on a water-soluble self-assembled DNA nanoarray carrying detection probes. The fluorescence enhancement upon the addition of specific detection targets was directly observed by confocal fluorescence microscopy. The versatility of the system was demonstrated by successful detection of SARS viral DNA and adenosine triphosphate (ATP). Improvement of sensitivity by two orders of magnitude was achieved for both targets, compared to our previously reported system without signal amplification. This work provides proof-of-concept that HCR can efficiently occur on DNA-tile based nanoarrays thus facilitating more sensitive detection. The merging of HCR with combinatorial encoding systems to realize highly sensitive and multiplexed biosensing may provide new tools for nanomedical applications.

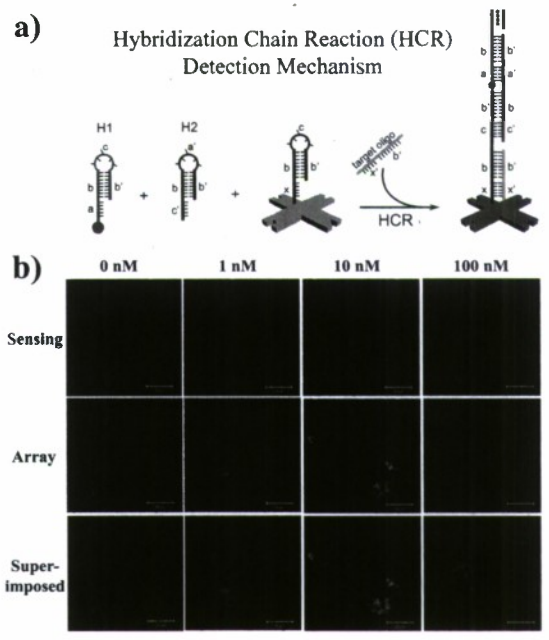

Figure 6. Detection of SARS viral DNA by employing HCR reaction on DNA-tile based arrays. **a)** Detection mechanism: A unique hairpin designed for the specific oligonucleotide target (SARS viral DNA) is incorporated on a DNA-tile that can self-assemble into two-dimensional arrays (not illustrated here). Two hairpins (H1 and H2), one of which (H1) is labeled by a red fluorescent dye (Rhodamine Red), are in the mixture with the DNA array. In absence of the target, the hairpins, either on-tile or in-solution, retain their close states. The addition of the oligonucleotide target opens the on-tile hairpins, triggering HCR reaction between H1 and H2, leading to the elongation of nicked DNA double helices on tiles and ultimately resulting in the accumulation of red fluorescence signals on DNA nanoarrays. Unique stretches of DNA sequences are denoted by lower case letters, in such a way that a' is the Watson-Crick complement to a, etc. **b)** Detection by confocal fluorescent microscope. The DNA array is at 200 nM concentration (DNA tiles) and pre-stained by YOYO-1 (green fluorescence) before imaging. The concentrations of SARS viral DNA are labeled above the corresponding images. Each sample is scanned through "green (array)" and "red (signal)" channels and the superimposed image is displayed in the bottom row. The detection limit is estimated to be 1 nM for the target. Scale bars: 20 μm.

HCR reaction is initiated by a single-stranded DNA (ssDNA) that opens one of the closed hairpins and starts the cascading hybridization. The ability of a small amount of ssDNA to trigger the assembly of a high molecular weight complex makes HCR a suitable candidate as a signal amplifier for biomolecular detection. Furthermore, all the components involved in HCR are simple oligonucleotides, which can be easily grafted onto DNA-tile based arrays. Finally, one or both of the hairpins can be modified with fluorophores, resulting in HCR products that are fluorescence-rich and capable of being read out by simple optical means.

We first tested the detection of SARS viral DNA by employing HCR reaction on DNA-tile

based nanoarrays. The design is schematically illustrated in Figure 6a. Here the HCR initiator is initially protected by a self-folded hairpin that is anchored on a cross-shape DNA-tile (detection tile). The sequence of this hairpin is precisely designed so that it will partially hybridize with SARS viral DNA and switch from a closed state to an open state to free the initiator. With this design, the on-tile HCR can be triggered by the addition of SARS viral DNA. In the presence of another cross-shape DNA-tile (linker tile, not shown in the schematic) with complementary sticky ends to the detection tile, the on-tile hairpins can be assembled into two-dimensional (2D) arrays with ~28 nm spacing between adjacent hairpins. Two additional hairpins (H1 and H2) are designed to facilitate cross-hybridization upon the de-protection of initiator. When HCR occurs, it leads to the elongation of nicked double helices on the array. H1 is labeled by a red fluorescent dye (Rhodamine Red). The net effect upon the addition of SARS viral DNA is the accumulation of a red fluorescent signal on the array, which can be directly visualized under fluorescent microscope.

A series of samples containing 200 nM sensing arrays and 0~100 nM SARS viral DNA was first stained by YOYO-1, a green fluorescent dye that intercalates into dsDNA, and then imaged using a confocal fluorescent microscope. In the absence of SARS viral DNA, no red fluorescence signal was observed. Upon the addition of SARS viral DNA with a concentration as low as 1 nM, the arrays start to appear red. The detection signal grew stronger with the addition of more targets, suggesting that the fluorescence color change is indeed due to the presence of target. It is interesting to note that at relatively low target concentrations (e.g. 10 nM), the HCR does not occur uniformly on every arrays, resulting in some arrays appearing a deeper red than the others. This is probably a result of the uneven opening of initiator hairpins on different arrays due to insufficient target amount. Nevertheless, the HCR happens exclusively on the self-assembled DNA arrays upon the addition of target. The detection limit here is estimated to be ~1 nM, which is approximately 100 fold more sensitive compared to detection using a similar design at the same array concentration without signal amplification.

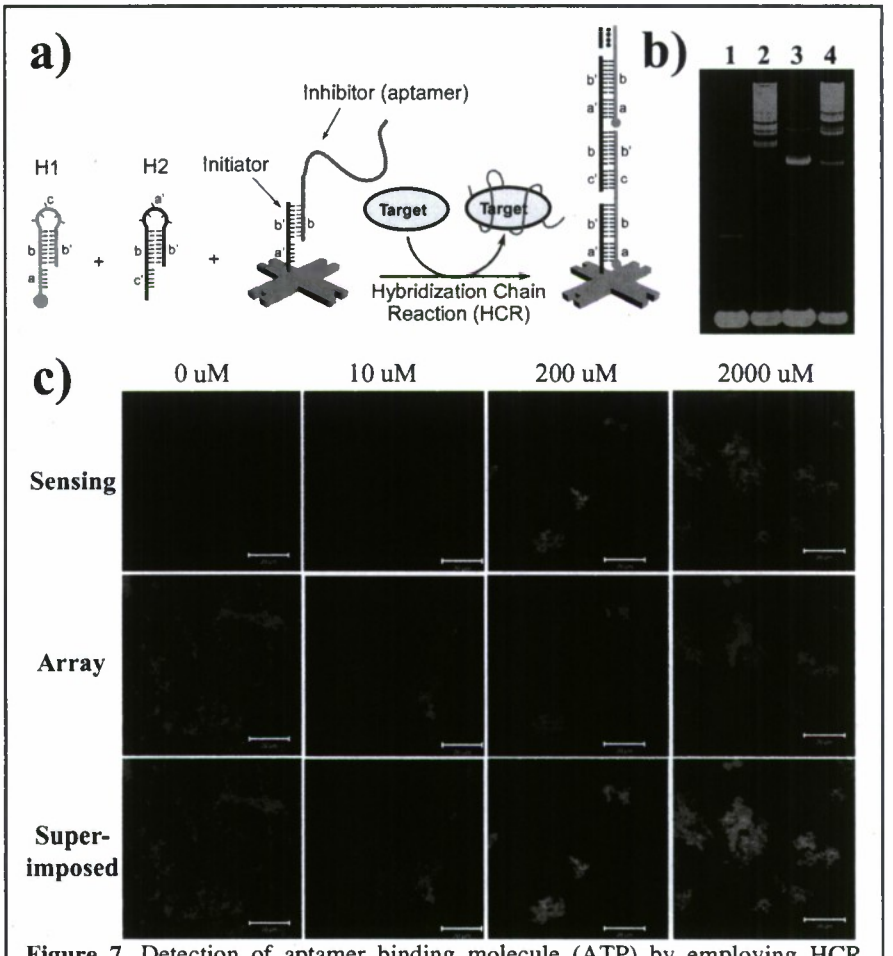

Figure 7. Detection of aptamer binding molecule (ATP) by employing HCR reaction on DNA-tile based nanoarrays.

It has been demonstrated that HCR can also be triggered by aptamer binding molecules (instead of DNA or RNA oligomers) if the initiator is properly protected by the aptamer of the detection target. This offers increased versatility of our sensing system. To investigate the possibility of detecting aptamer binding molecules, we chose adenosine triphosphate (ATP) as a model target. The design for ATP detection is very similar to the design for SARS virus detection, with two alterations (Figure 7a).

First, instead of having the initiator protected as a hairpin, an ssDNA inhibitor comprising the sequence of the ATP aptamer is partially hybridized to the initiator to inhibit the HCR reaction before target addition. Such a design ensures that the free end of the aptamer protrudes out from the tile plane granting a better access for ATP. When ATP is present, it will bind to the aptamer and cause strand displacement. This will expose the bare initiator on the detection tile, which triggers HCR between the hairpins. Second, H1 is labeled by a green fluorescent dye (Alexa Fluor 488) rather than red, and as an accommodation, the linker tile (not shown in schematic) is labeled with a red fluorophore (Cy5) to assist with the observation of the DNA arrays without the occurrence of HCR.

To validate the altered design, we first tested the HCR in solution (without tile) by non-denaturing polyacrylamide gel electrophoresis (PAGE, Figure 7b). An excessive amount of inhibitor (2x) was added to ensure minimal leakage reactions in the absence of ATP. From the PAGE assay, the HCR reaction was inhibited to a very low level before the addition of ATP (Figure 7b, lane 3). In the presence of 2 mM ATP, HCR occurs at the same level as when the hairpins (H1 and H2) are directly exposed to the un-protected initiator, represented by high molecular weight products with strong fluorescence (Figure 7b, lane 2 and 4). For the fluorescence imaging, increasing amounts of ATP (0~2000 μM) were titrated against 1 μM ATP sensing arrays (Figure 7c). Although there was background signal without any ATP in the solution (which is in agreement with the findings by PAGE assay), the fluorescence color change in response to 10 μM ATP was significant enough to be clearly distinguished from the leakage. It is worth noting that the dissociation constant (K_d) between ATP and the structure-switching aptamer probe used here is about 600 μM. Therefore, a detection limit approximately 2 orders of magnitude lower than the probe's K_d value shows the power of signal amplification brought by HCR.

In summary, we have successfully constructed a self-assembled DNA-tile-array based biosensor with improved sensitivity compared to its ancestor. The introduction of HCR as a signal amplifier enables a small amount of target to trigger a significantly increased fluorescence signal that is confined locally to be observed by fluorescence microscopy. The signal amplification is achieved through HCR reaction by forming a long linear molecule at the target binding site located on a DNA array, which concentrates the fluorescent dye labeled DNA hairpins that freely diffuse in solution onto a DNA array immobilized on a surface, making the signal change easily visible under a microscope. Efficient detection can be achieved at low target to probe ratios (e.g. 1:200). The on-tile HCR assay presented here is highly reproducible. Quantitative data can be acquired from fluorescence microscope images.

In principle, by only altering the probe and hairpin sequences, this design can be easily adapted to detect other oligonucleotides with varying lengths and sequences, as well as other aptamer binding molecules such as proteins. When altering the design, it is crucial for the hairpin probes to have proper length stems and loops so that they are stable at room temperature in the absence of target, but can efficiently facilitate polymerization in the presence of analyte. It has been demonstrated that hairpins with loop length of 6-nt and stem length of 18-bp perfectly meets this criteria. Therefore, when other nucleic acid targets are encountered, it is reasonable to maintain the same secondary structure of all hairpins and change only the anchored hairpin on-tile so that it can be opened by the target strand and free the initiator. For example, if HIV virus DNA (39-nt) needs to be detected, the anchored hairpin must be re-designed with its stem(18-bp)-loop(6-nt) structure maintained and single stranded anchor elongated (11-nt). Obviously, the sequences of all hairpins (H1 and H2) must be changed accordingly. The work presented here utilized assorted fluorophores with well-separated spectra (Alexa fluor 488 and Rhodamine Red) to signal various targets (ATP and SARS viral DNA). This leads us to believe that this signal amplification strategy can be used in multiplexed sensing systems to realize highly sensitive detection of multiple biomolecules simultaneously. Using a combinatorial encoding strategy, the multiplexing capability of such a system is expected to be considerably high, limited only by the ability of the fluorescence microscope to differentiate the relative fluorescence intensity levels. In the future, this system can be further improved by utilizing quantum-dots with narrower emission spectra and brighter photoluminescence relative to organic dyes as fluorescent labels.

2.4 Self-assembled DNA nanoarrays for single molecule protein capturing and detection through optimized multivalent binding

To further improve the DNA nanoarray based detection capability, it is important to develop strategies that can enhance the binding affinity of the potential targets (e.g. proteins) to the functional ligands on the self-assembling DNA nanoarray. We have been made significant progress in this direction by designing and constructing distance dependent multivalent binding to capture protein targets with higher affinity and image the binding event at single molecule level.

Various approaches have been developed to engineer multivalency by linking multiple ligands together. However, the effects of well-controlled inter-ligand distances on multivalency are less understood. Recent progress in self-assembling DNA nanostructures with spatial and sequence addressability has made deterministic positioning of different molecular species possible. Here we show that distance-dependent multivalent binding effects can be systematically investigated by incorporating multiple affinity ligands into DNA nanostructures with precise nanometer spatial control. Using atomic force microscopy, we demonstrate direct visualization of high affinity bivalent ligands being used as pincers to capture and display protein molecules on a nanoarray. These results illustrate the potential of using designer DNA nanoscaffolds to engineer more complex and interactive biomolecular networks.

The model system (Fig. 8) we chose to demonstrate the distance-dependent multivalent ligand-protein binding consists of two different aptamers positioned into a multi-helix DNA tile to bind a single protein target, such that the distance between them can be precisely controlled by varying the spatial arrangement of the aptamers on the DNA tile. Aptamers are oligonucleotide-based recognition regions that are selected to bind small molecules or proteins. Both aptamers used here are thrombin (a coagulation protein involved as a key promotor in blood clotting) binding aptamers which have been previously selected and well characterized. Each aptamer has a unique sequence and binds to a nearly opposite site on the thrombin molecule. Aptamer A (apt-A: 29 mer, 5'-AGT CCG TGG TAG GGC AGG TTG GGG TGA CT-3') binds to the heparin binding exosite, and aptamer B (apt-B: 15 mer, 5'-GGT TGG TGT GGT TGG-3') binds primarily to the fibrinogen-recognition exosite. We hypothesized that, by varying the length of a rigid spacer, an optimal inter-aptamer distance will be achieved such that the two aptamers will act as a bivalent single molecular species that displays a stronger binding affinity to the protein than any one of the individual aptamers does alone.

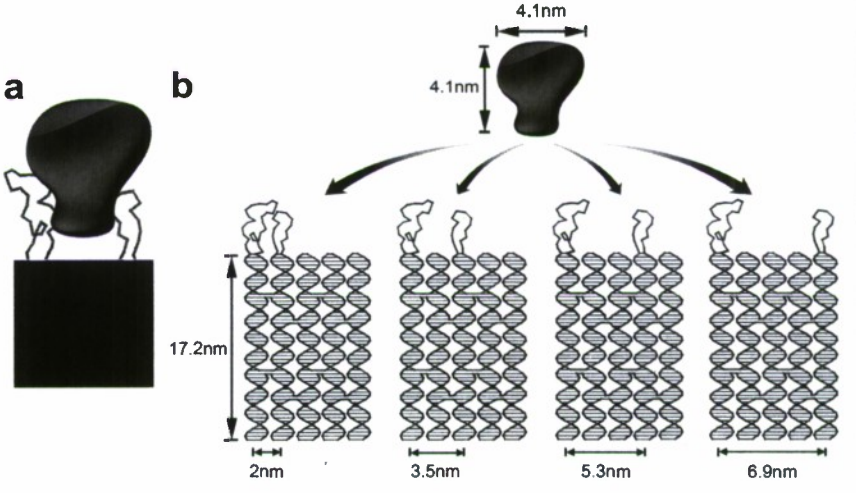

Figure 8. Schematics of the self-assembled divalent aptamers on DNA tile for protein binding. a, A cartoon showing a rigid DNA tile (blue) that can spatially separate two ligands (red and green) at a controlled distance with each ligand attached to a different part of the target molecule (orange) for bivalent binding. **b,** 5-helix-bundle (5HB) DNA structure with apt-A (red) and apt-B (green) protruding out of the tile helices and being separated at a distance of 2, 3.5, 5.3, and 6.9 nm. The aptamer sequences were incorporated into the closed loops extending out of the ends of the helices. Apt-A is fixed on helix 1 and apt-B is moved between helix 2 and helix 5, generating the varying inter-aptamer distances but keeping the relative orientations constant. Numbering of the helices in the tile is read from left to right.

The multi-helix DNA tile was designed and constructed from either a four-helix bundle (4HB) structure or a five-helix bundle (5HB) structure (generated by narrowing an eight-helix bundle tile) that was modified with the closed-loop aptamer sequences extending out from the ends of the helices (Fig. 7b). The spacing between the two aptamers can be controlled with subnanometer precision. For example, the 5HB DNA tile can provide 2, 3.5, 5.3 and 6.9 nm inter-aptamer distances. This was accomplished by integrating apt-A into helix 1 (the left-most helix) and moving apt-B from helix 2 to 5 (to the right). The relative axial orientation of the two aptamers was kept the same at all inter-aptamer distances.

We used gel-mobility shift assays to reveal the optimal spacing between apt-A and apt-B for bivalent binding. Due to their smaller size, the 4HB-tile-based bivalent aptamers would give a more obvious mobility shift during gel electrophoresis when bound with thrombin, compared to that of the 5HB tiles. The 4HB tiles carrying aptamers at various spacings (2, 3.5 and 5.3 nm intervals) were incubated with and without thrombin (40 nM protein, [DNA tile]:[protein] = 1:2) before they were analyzed using non-denaturing PAGE (see methods and Supplemental Information).

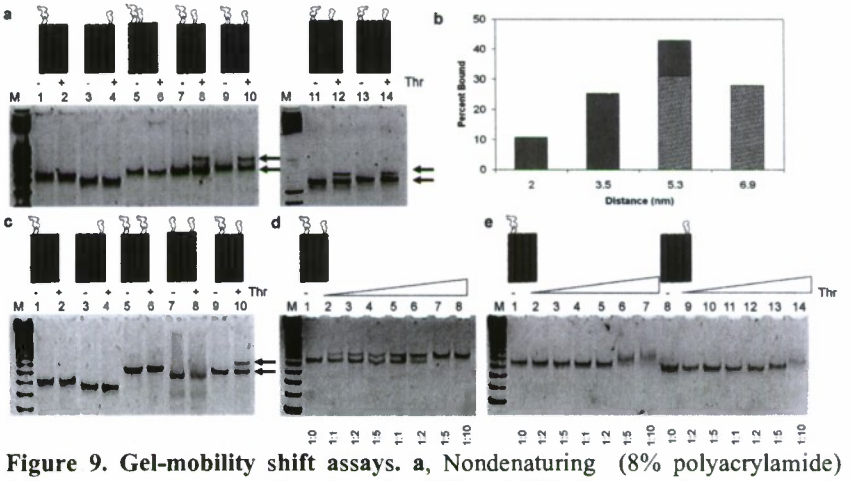

Figure 9. Gel-mobility shift assays. a, Nondenaturing (8% polyacrylamide) PAGE image of aptamers linked on the 4HB and 5HB tiles. Lane M corresponds to a 25bp DNA marker. Lanes 1 to 14 correspond to 4HB-A1, 4HB-B4, 4HB-A1-B2 (2 nm), 4HB-A1-B3 (3.5 nm), 4HB-A1-B4 (5.3 nm), 5HB-A1-B4 (5.3nm), and 5HB-A1-B5 (6.9 nm), each 20 nM without (-) and with (+) thrombin (40 nM), respectively. The lower band in each lane represents the unbound tiles and the upper band in lane 6, 8, 10, 12 and 14 represents the tile/thrombin complex. **b**, The dependence of protein binding on the inter-aptamer distance. Here 20 nM 4HB or 5HB tiles containing both apt-A and apt-B with varying distances were incubated with 40 nM thrombin before they were loaded into the gel. The percentages of bound DNA tiles were estimated from the relative intensity of the bands in the gel image shown in panel a. The filled bar and striped bars are data from the 4-HB and 5-HB tiles respectively. **c**, The binding of thrombin to the 4HB tile-based aptamer structures carrying one aptamer or two of the same or different aptamers. All tiles with two aptamers have the same inter-aptamer distance at 5.3 nm. Lane M corresponds to a 25 bp DNA marker. Lanes 1, to 10 correspond to 4HB-A1, 4HB-B4, 4HB-A1-A4, 4HB-B1-B4, and 4HB-A1-B4 without (-) and with (+) thrombin (40 nM). An upper band is only observed in lane 10 with 4HB-A1-B4 (same as lane 10 in panel a). **d**, Titration experiment showing more DNA tiles (4HB-A1-B4, 1 nM) are bound to the protein with increasing concentrations of thrombin. Lane M corresponds to a 25 bp DNA ladder. From this gel a 10 nM apparent K_D is estimated for the bivalent binding of thrombin to the two aptamers linked by a DNA tile at a 5.3 nm distance. **e**, Titration experiment for 4HB-A1 (lanes 1-7) and 4HB-B4 (lanes 8-14). Lane M is a 25 pb DNA ladder. From this gel, the apparent K_D for the two individual aptamers on the 4HB tile are estimated to be 20-50 nM and > 50 nM, respectively.

The 4HB tile containing only apt-A on helix 1 (4HB-A1) and the 4HB tile containing only apt-B on helix 4 (4HB-B4) serve as controls, which both show no slower migrating band when incubated with thrombin (Fig. 9a lanes 1-4) at this concentration. The dissociation constants (K_D) of these two aptamers with thrombin have been determined to be sub-nM or 75-100nM, respectively. There are also variations of the K_D in literature depending on the different methods used. In the gel mobility assay, the binding complexes are at non-equilibrium while migrating through the gel. Therefore the apparent dissociation constant K_D measured here is expected to be much larger than the solution K_D measured under equilibrium conditions. This can explain the observed low affinity of these two aptamers acting alone.

When tiles are incubated with thrombin and carry two differing aptamers at a distance of 2nm (4HB-A1-B2), a very faint significantly slower migrating band can be seen, representing a small population of the DNA structure binding to thrombin (Fig. 9a lanes 5 and 6). From the significant lagging position of the band, we propose that in this binding complex, each thrombin molecule is sandwiched by two aptamers from two individual tiles. At a distance of 3.5 nm (4HB-A1-B3), another distinct upper band appears closely above that of the DNA tiles. We propose that this band is due to the binding of one thrombin molecule by the two different aptamers on the same DNA tile (Fig. 8a lanes 7 and 8), i.e. the bivalent binding. It is estimated from the relative intensities of the upper and lower bands that ~ 25% of the structure is bound to thrombin. At a distance of 5.3 nm (4HB-A1-B4), the relative intensity of this band increases, and ~ 40% of the structure is bound with thrombin (Fig. 8a lanes 9 and 10). Further, we used 5HB to generate a 6.9 nm spacing between the aptamers. The gel mobility shift assay (Fig. 9a lanes 11-14) showed a decreased binding at 6.9 nm spacing (5HB-A1-B5) compared to 5.3 nm spacing (5HB-A1-B4). Since the size of the thrombin protein is ~ 4 nm, we did not expect to see improved binding at any larger distances greater than 6.9 nm.

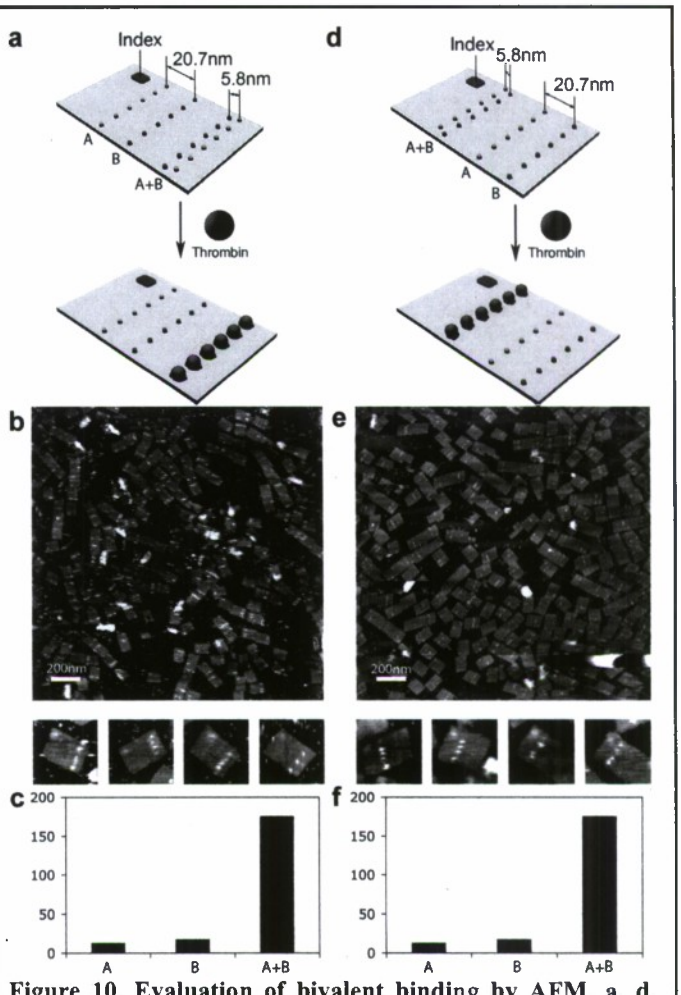

Figure 10. Evaluation of bivalent binding by AFM. a, d, schematic drawings of two rectangular-shaped DNA origami tiles containing two lines of apt-A (green dots) and two lines of apt-B thrombin (blue dots). The neighboring lines of apt-A and apt-B are ~ 20.7 nm (marked line A and line B) and ~ 5.8 nm (line A+B) apart. We call the closely spaced lines the dual-aptamer line. An index is also included helping to verify the positions of the lines in the AFM images. **b, e,** AFM height images of the DNA origami tiles (10nM) with 60 nM thrombin, corresponding to **a** and **d,** respectively. Zoom-in images are 150nm x 150nm. **c, f,** Charts of numbers of proteins binding on each aptamer line (observed from 60 arrays corresponding to **a** and **d** respectively). Bar A represents the number of proteins on the line of apt-A, bar B represents the number of proteins on the line of apt-B, and bar A+B represents the number of proteins on the bivalent dual aptamer line.

The percent of protein-bound DNA tiles at the different spacings were estimated based on the gel shift assay in Fig 9a, and plotted in Fig 8b. It is noted that, for the same distance arrangements (5.3 nm), the thrombin binding affinity of the bivalent aptamers on 5HB was slightly lower than that on 4HB. This difference is possibly due to the effect of an extra helix on the 5HB tile that might limit the rotational freedom of the aptamer on the 4th helix. Overall, the inter-aptamer distance at 5.3 nm was determined to be optimal for the bivalent binding (Fig. 9b).

As a control experiment to show that only hetero-aptamers can give such bivalent binding capability, we compared the binding of the tile containing two identical aptamers arranged at the same 5.3 nm distance, 4HB-A1-A4 and 4HB-B1-B4, with the tile containing two different aptamers (4HB-A1-B4). As shown in Fig. 9c, only the tile with the hetero-aptamers displayed an upper band when incubated with thrombin (lane 10). The homo-dimers did not show any significant binding, similar to the monomers. This result clearly indicated that the increased binding affinity is not caused by the increase in the number of aptamers per structure, but

rather because of the type of aptamers that have a bivalent binding capability. We believe that the two hetero-aptamers act together as a pincer to grab the same thrombin molecule; each attaching to a different site on the protein. Such nano-pincers are able to bind thrombin tightly but can be made to release their ligands when triggered by an external chemical signal, i.e. by adding the oligonucleotide complementary to the aptamer.

One unique feature in our aptamer loop design is that we added four thymine bases at the end of the stems on both strands of the helix, thereby increasing their 3-dimensional flexibility. Both aptamer sequences are known to have a stem/binding region, utilizing only a few bases for contact with the surface of thrombin. In order to find an optimal relative orientation of the two aptamers, we tried to rotate apt-B on the 4HB-A1-B4 by 90° and 180° by adding three or six base pairs to the stem, respectively. Both show a slight decrease in binding efficiency in comparison to the original design of 4HB-A1-B4 (Fig. 9d), however no obvious difference between these two structures was observed. We propose that the 3- dimensional flexibility provided by the TTTT on the stems enables both aptamers to rotate in a limited range that can compensate for small changes in the center-to-center distances between the two aptamers so that bivalent binding efficiency can be maximized.

A rough estimate of the binding affinity of 4HB-A1-B4 to thrombin was obtained by titration of the thrombin concentration in the gel mobility shift assay (Fig. 9d lanes 1-8); a K_D of ~ 10 nM was obtained. This is about 10 fold increase in affinity compared to those of the individual apt-A or apt-B on 4HB (4HB-A1 and 4HB-B4, in Fig. 9e lanes 1-14), whose K_D was estimated to be 20-50 nM and > 50 nM, respectively. These titration results confirmed that the bivalent binding of the hetero-aptamers placed at the optimized distance can have a binding affinity better than any of the monovalent binding.

We also attempted to adapt a solution based method previously developed to measure the binding affinity of the aptamer to thrombin using a molecular aptamer beacon (MAB). A K_D of the 15-mer MAB was reported as 5.2 nM. Using the same MAB, we observed effective displacement of the thrombin from the MAB by the 4HB-tile based bivalence aptamer 4HB-A1-B4. From this displacement experiment, we estimated that the tile-based bivalence aptamer binds to thrombin about ~ 50 fold stronger than the 15-mer aptamer does and has a solution K_D of ~ 0.1 nM.

Atomic force microscopy (AFM) was also used to study the bivalent binding of these two aptamers at the single molecular level. Using the DNA origami method we designed a rectangular-shaped DNA tile (Fig. 10a) that had a dimension of 60 x 90 nm. Stem-loops with apt-A and apt-B sequences were designed to protrude out of the plane of the DNA origami tile. We put two lines of each aptamer (for a total of four lines of aptamer probes) on the DNA origami tile, with a distance of ~ 20.7 nm and ~ 5.8 nm between the neighboring lines of apt-A and apt-B, and an intra-line distance of ~ 12 nm for the same aptamer. Based on the estimated K_Ds, when we add a 1:4 ratio of thrombin to the total number of aptamers, no or low binding is expected on the lines that are further apart, while stronger binding is expected on the bivalent dual-aptamer lines (marked as A+B in Figure 10a). A group of 6 closely-placed dumb-bell loops that provide a height contrast under AFM imaging was positioned in one corner of the tile as a topographic index reference to unambiguously determine the relative positions of each aptamer line.

To rule out the possibility of positional effects due to electrostatic repulsion between the probes and the DNA scaffold, the positions of the dual-aptamer lines were switched from close to one side of the tile to the middle on another DNA origami tile (Fig. 10d). AFM images (Fig. 10b, 10e) showed that thrombin preferred to bind to the dual aptamer lines on both DNA origami tiles. Individual protein molecules can be distinctly detected. We counted the number of protein molecules bound to each aptamer line (Fig. 10c, 10f). The dual-aptamer line shows a ~10 fold better protein binding than the single aptamer lines, consistent with the gel assay results.

This study represents the first example of utilizing the spatial addressability of self-assembled DNA nanoscaffolds to control multi-component biomolecular interactions and to visualize such interactions at a single molecule level. In addition to aptamers, one may be able to position small peptides, sub-domains and cofactors of enzymes, or carbohydrate molecules into 2D and 3D spatially controlled networks to obtain multivalent behavior, which may be used to probe sterical constraints,

ionic interactions and hydrophobic interactions. It may also be possible to use addressable DNA nanoscaffolds to position motor proteins at a particular inter-molecular distance to display complex motor behaviors on a well-defined nanoscale landscape, generated for example, by modifying the staple strands of the origami at different locations.

2.5. Improving photostability of the fluorescent encoded DNA nanoarrays using quantum dots

One of the original goals of this YIP project was to develop self-assembling nanoarrays to contain fluorescent labels that are photostable so it can become a more robust platform for detection. In this direction we have been successful assembled streptavidin coated QDs onto DNA nanoarrays through biotin-streptavidin interaction and tested the photostability of the DNA templated QD arrays.

To our knowledge, there has been no prior report demonstrating DNA tile directed self-assembly of semiconducting NPs (QDs) into rationally designed architectures, partly may be due to the significantly different surface properties of QDs and gold NPs. Herein, we worked out a strategy to use two-dimensional DNA tile arrays to direct the assembly of streptavidin conjugated CdSe/ZnS core/shell QDs into well-defined periodic patterns.

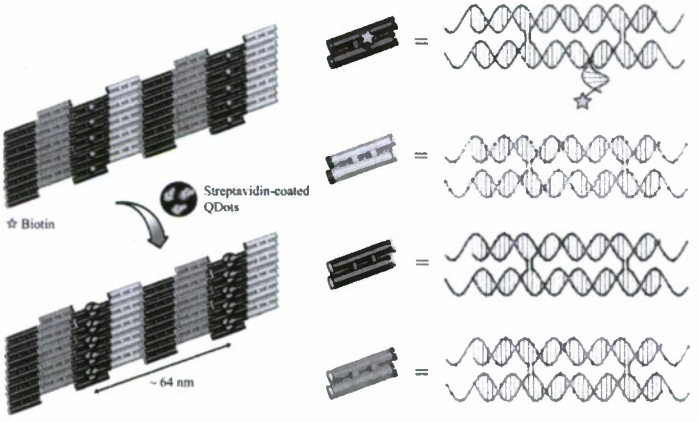

Figure 11. Schematic showing the process of DNA tile directed self-assembly of QD arrays.

The strategy and schematic process of the DNA tile directed QD assembly is illustrated in Figure 11. We used a set of four double crossover (DX) molecules, named the ABCD tile system, as scaffolds for QD assembly. Each different DX tile (DX-A, DX-B, DX-C and DX-D) is shown by a different color in Fig. 11. The 'A' tile contains a short DNA stem protruding out of the tile plane that carries a biotin group (illustrated as yellow star) at the end. Upon self-assembly, the four-tile system gives 2D arrays displaying parallel lines of biotin groups, with a periodic distance between two neighboring biotin lines ~ 64 nm, and a distance between two biotins within the line about 4-5 nm. After adding streptavidin coated CdSe/ZnS QDs (Invitrogen, Qdot® 545 ITK™ streptavidin conjugate, or STV-QD) to the DNA array, streptavidin molecules (illustrated as yellow blocks) specifically bind to the biotin groups so that the QDs (illustrated as black ball) will be organized onto the DX tile arrays.

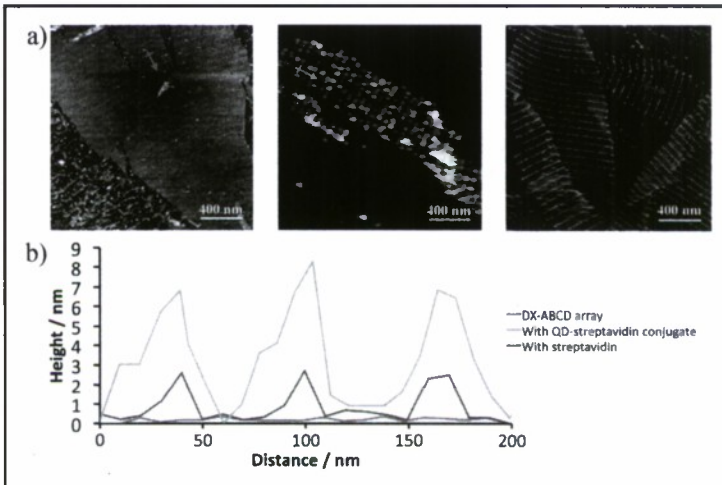

Figure 12. a) From left to right: AFM images of DX-ABCD array alone with each A tile bearing a biotin; the biotinylated DX-ABCD array incubated with STV-QD conjugate; and same array incubated with streptavidin only; b) Cross section analysis of the AFM images. Each trace corresponds to the same colored arrow in a).

AFM images and cross-section profiles shown in Figure 12 clearly demonstrate that STV-QDs bind specifically to the DX array and get organized into periodical stripes of QD arrays with the designed distances between the parallel lines. Due to the short stem on A tile carrying the biotin group, the patterned 2D array of the ABCD tile system alone (left image and blue trace)

show a small height change across the line of the biotin groups, ~ 0.5 nm. When STV-QDs bind to the DX array (middle image and green trace), the average height across the biotin sites increases to ~ 9 nm. A control experiment by adding streptavidin to the same type of biotin modified DX arrays shows a height change of only ~ 2 nm (right image and red trace). The height change resulting from the STV-QD binding is significantly higher than that of streptavidin binding to the array, the line widths are also much wider, owning to much larger sizes of the STV-QDs (diameter estimated ~ 10 nm including the surface polymer and protein coating), compared to that of the protein molecules alone ~ 2-3 nm.

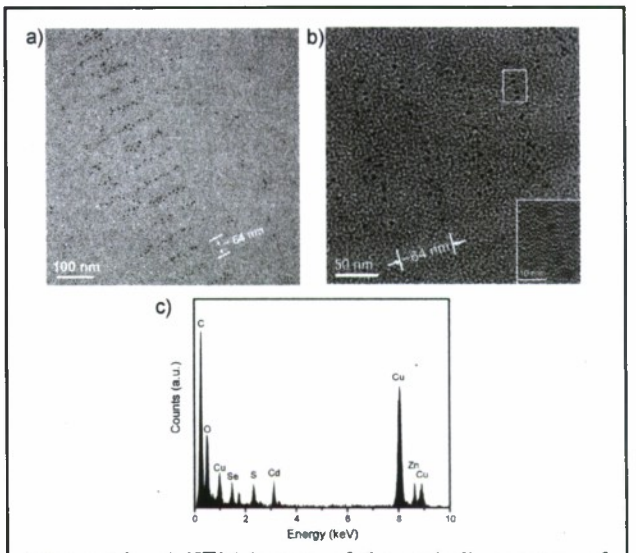

Figure 13. a) TEM images of the periodic patterns of the organized QD arrays. b) High resolution TEM images with an insert in the right corner reveal the crystalline structure of the QDs. c) EDX spectrum verifies the composition of the CdSe/ZnS QDs.

TEM imaging further reveals the patterning of QD arrays templated by the DX tiles. TEM images shown in Figure 13 represent the periodic alignment of QDs into parallel stripes with measured periodicity of ~ 64 nm between the lines, matched well with the designed paramcters. The diameter of each individual QD particle is measured ~ 4 nm, corresponds to the size of CdSe/ZnS QDs with green emission. The protein and polymer coating on the surface of the QDs are not visible due to low electron density thus low contrast in the TEM image. It is notable the QDs within each stripe sometimes slightly shift out of the line, which may be due to the orientational flexibility of the short protruding DNA stems bearing the biotin group and the tendency of neighboring QDs to avoid steric crowdedness. The ccnter to center distance between QDs within the same line measures from 7 to 15 nm, which is larger than the distance between neighboring biotin groups, 4-5 nm in the DX array. This can be explained by the large size of the protein coated QDs causing steric hindrance within the line. In addition, the multiple streptavidin molecules conjugated on each QD and the multivalency of streptavidin-biotin binding may also contribute to this effcct. It is possible that multiple streptavidin molecules on a single QD may obtain orientations that allow for binding of two or three neighboring biotin groups in the same line. Taking the size of the QD with the protein and polymer coating on surface into account, this 7-15 nm distance is close to the highest possible packing density of the protein coated QDs in the line.

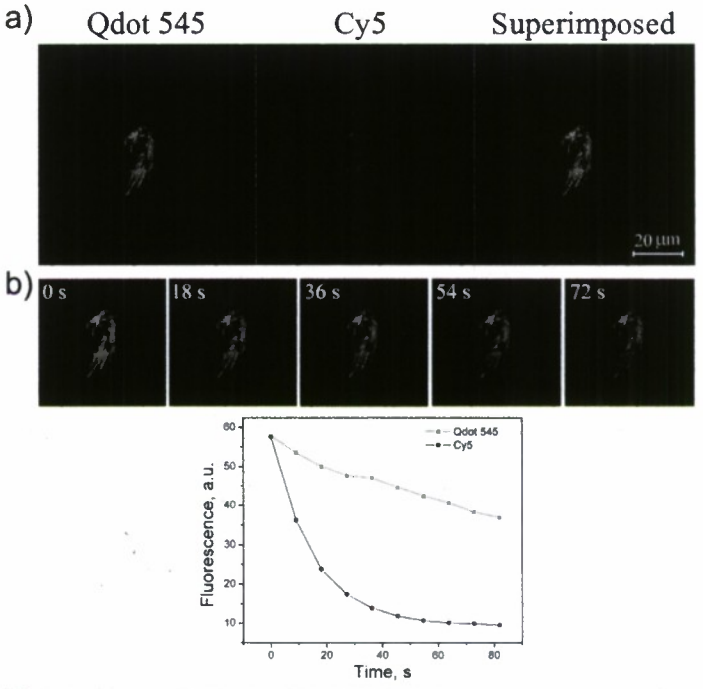

Figure 14. a) Confocal fluorescent microscope images and b) photobleaching on the DNA arrays. Scale bar: 20 μM.

High resolution TEM images (insert in Fig. 13b) clearly reveals the crystalline structure of the QDs and the energy dispersive X-ray (EDX) data supports that the NPs in the image are composed of CdSe/ZnS, as shown in Figure 12c.

In addition to AFM and TEM imaging, we further used laser fluorescence imaging and photo-bleaching experiments to demonstrate that the QDs were assembled onto the DX array. In this experiment, a DNA strand in the B tile of the DX array was modified with an organic fluorophore with red emission, Cy5 (l_{em}= 648 nm). The DX arrays carrying both Cy5 and STV-QD of green emission (l_{em}= 545 nm) was imaged by fluorescence imaging (Figure 14a), revealing the co-localization of red Cy5 and green QDs on the DNA array (see superimposed fluorescent image in Fig. 13a, rightmost panel). It is well-known that QDs have higher photostability than organic fluorophores. A rectangular shaped region of 11x15 μm^2 was selected from the imaged area to be photobleached (Fig. 14b). This region was constantly irradiated by a focused 405 nm laser beam at the power of 0.9 mW for 81 s. Images were taken using the same sequential scanning set-up with 9 s intervals during the photobleaching process. The change of the relative intensity of the red and green fluorescence in the bleached region was also plotted in Figure 14b. It is clear that the organic fluorophore was photobleached with a 90% drop of intensity within 30 s, while the emission intensity of the green QDs still persists after 80 s. This experiment further indicates that QDs are successfully organized onto the DNA tile arrays.

2.5. Photostable Combinatorial Encoding DNA nanoarrays using Quantum Dots as labels

To construct combinatorial encoding nanoarrays using QDs as photostable fluorescent labels. We tested the combinatorial assembly of QDs of two different colors (red and green emission) on DNA nanoarrays. Figure 15 shows the conforcal fluorescent microscope images of a series of combinatorial encoding nanoarrays assembled using DNA tiles as templates and green and red streptavidin coated QDs (from Invitrogen) by varying the stoichiometry ratios between the two different QDs. This is the first example of using self-assembling DNA tile nanoarrays to direct the formation of combinatorial QD nanoarrays, fulfilling our original goals listed in the project.

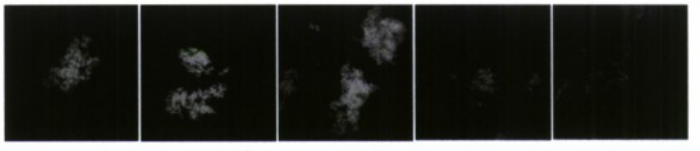

Figure 15. Confocal fluorescent microscope images of barcode arrays generated by sampling different ratio of QDs on DNA arrays. From left to right: 4G0R; 3G1R; 2G2R; 1G3R; 0G4R. Each image is 90 um x 90 um scale. G represents green colored QD and R represents red colored QD.

Publications Produced:

1. R. Chhabra, J. Sharma, Y. Ke, Y. Liu, S. Rinker, S. Lindsay, **H. Yan,** Spatially Addressable Multi-protein Nanoarrays Templated by Aptamer Tagged DNA Nanoarchitectures, ***J. Am. Chem. Soc.*** 129, 10304-10305 (2007).

2. C. Lin, Y. Liu, **H. Yan*,** Self-assembled Combinatorial Encoding Nanoarrays for Multiplexed Biosensing, ***Nano Lett.*** 7, 507-512 (2007).

3. Y. Ke, S. Lindsay, Y. Chang, Y. Liu, **H. Yan,** Self-assembled Water-soluble Nucleic Acid Probe Tiles for Label Free RNA Detection, ***Science*** 319, 180-183 (2008).

4. Y. Ke, J. Nangreave, **H. Yan**, S. Lindsay, Y. Liu, Developing DNA tiles for oligonucleotide hybridization assay with higher accuracy and efficiency, ***Chem. Commun.*** 5622-5624 (2008).

5. C. Lin, J. Nangreave, Z. Li, **H. Yan**, Y. Liu, Signal Amplification on a DNA Tile based Biosensor with Enhanced Sensitivity, ***Nanomedicine*** 3, 521-528 (2008).

6. S. Rinker, Y. Ke, Y. Liu, **H. Yan,** Self-assembled DNA Nanostructures for distance dependent multivalent ligand-protein binding, ***Nature Nanotechnology*** 3, 418-422 (2008).

7. J. Sharma, Y. Ke, C. Lin, R. Chhabra, Q. Wang, J. Nangreave, Y. Liu, **H. Yan**, DNA Tile Directed Self-assembly of Quantum Dots into Two-dimensional Nanopatterns, ***Angew. Chem. Int. Ed.*** 47,

5157-5159 (2008).
8. Q. Wang, Y. Liu, Y. Ke, **H. Yan,** Quantum Dots Bioconjugation During Core-Shell Synthesis, ***Angew. Chem. Int. Ed.*** 47, 316-319 (2008).
9. C. Lin, S. Rinker, X. Wang, Y. Liu, N. C. Seeman, **H. Yan**, In-vivo Cloning of DNA Nanostructures, ***Proc. Natl. Acad. Sci. USA*** 105, 17626-17635 (2008).
10. Z. Li, B. Wei, J. Nangreave, C. Lin, Y. Liu, Y. Mi*, **H. Yan***, A Replicable Tetrahedral Nanostructure Self-assembled from a Single DNA Strand, ***J. Am. Chem. Soc.*** 131, 13093-13098 (2009).
11. C. Lin, Y. Liu, H. Yan*, Designer DNA Nanoarchitectures, ***Biochemistry,*** *48, 1663-1674* (2009).
12. R. Chhabra, J. Sharma, Y. Liu, S. Rinker, H. Yan*, DNA Self-assembly for Nanomedicine, ***Advanced Drug Delivery Reviews*** (In press, 2010).

Scientific and technology transitions: Two patents applications are filed based on results produced from this project: US20100009868 Self-Assembled Combinatorial Encoding Nanoarrays for Multiplexed Biosensing; US20090297448 Quantum Dot Barcode Structures and Uses Thereof.

Invited presentations from 2007-2009:

1. "Designer DNA Nanostructures for Nanobiotechnology", Biophysics Seminar, Dept. of Physics and Astronomy, Rice University, Houston, TX, Nov. 6, 2009.
2. "Designer DNA Nanostructures for Nanobiotechnology", nanoUtah2009: 5th Annual Utah Statewide Nanotechnology Conference, Salt Lake City, Utah, Oct.16, 2009.
3. "Designer DNA Nanostructures for Nanobiotechnology", Dept. of Chemical and Nuclear Engineering, U. of New Mexico, Albquerque, NM, Sept. 29, 2009.
4. "Designer DNA Nanostructures for Nanobiotechnology", DNA Nanotechnology workshop, National Center for Nanoscience and Technology, Beijing, July 16, 2009.
5. "Designer DNA Nanostructures for Nanobiotechnology", Dept. of Chemistry, Univ. of Science and Technology of China, Hefei, July 10, 2009.
6. "Designer DNA Nanostructures for Nanobiotechnology", Institute of Applied Physics, CAS, Shanghai, July 8, 2009.
7. "Designer DNA Nanostructures for Nanobiotechnology", Materials Science and Engineering Department, Iowa State University, Ames, IA, April. 9, 2009.
8. "Designer DNA Nanostructures for Nanobiotechnology", Mini-symposium of Center for DNA Nanotechnology, Duke University, Durham, NC, March. 20, 2009.
9. "Designer DNA Nanostructures for Nanobiotechnology", Department of Chemistry, Florida State University, Tallahassee, FL, Feb. 27, 2009.
10. "Designer DNA Nanostructures for Nanobiotechnology", Joint MIT and Harvard Inorganic Chemistry Seminar Series, Department of Chemistry, MIT, Cambridge, MA, Jan. 21, 2009.
11. "Designer DNA Nanostructures for Nanobiotechnology", Departments of Material Science and Mechanical Engineering , UC Santa Babara, Santa Babara, CA Oct. 31, 2008.
12. "Designer DNA Nanostructures for Nanobiotechnology". the Joint Symposium of 18th International Roundtable on Nucleosides, Nucleotides and Nucleic Acids (IRTXVIII) and 35th International Symposium on Nucleic Acids Chemistry (SNAC), Kyoto, Japan, September 8th – 12th, 2008.
13. "Designer DNA Nanostructures for Nanobiotechnology". SPIE Optics and Photonics Meeting (Biosensing Symposium), San Diego, CA, August 10-14, 2008.
14. "Structural DNA Nanotechnology: Information Guided Self-assembly", Gordon Research Conference, Session on Bioorganic Chemistry (Organizer: W. A. Van Der Donk & P. L. Richardson), Andover, NH, June. 15-20, 2008.
15. "Designer DNA Nanostructures for Nanobiotechnology". Conference of International Materials and Technologies (CIMTEC08: Symposium E), Sicilly, Italy, June 8-13, 2008.

16. "Designer DNA Nanostructures for Nanobiotechnology". International Symposium for DNA based nanodevices, Jena, German, May 29-30, 2008.
17. "Designer DNA Nanostructures for Nanobiotechnology". Foundations of Nanoscience: Self-assembled Architectures and Devices (FNANO08), Snowbird, Utah, April 22-25, 2008.
18. "DNA based Nanscale Scaffolds, Assembly and Molecular Robotics". Office of Naval Research Workshop on DNA based Nanofabrication, Washington DC, April 11, 2008.
19. "Designer DNA Nanostructures for Nanobiotechnology". 3rd Annual Arizona Nanotechnology Cluster Symposium, Scottsdale, AZ, April 10, 2008.
20. "Designer DNA Nanostructures for Nanobiotechnology". Department of Chemistry, Texas A &M University, College Station, TX, April 4, 2008.
21. "Structural DNA Nanotechnology: Information Guided Self-assembly", Department of Chemistry and Biochemistry, Brigham Young University, Provo, Utah, March. 27, 2008.
22. "Designer DNA Nanostructures for Nanobiotechnology", 2008 William H. Nichols Symposium, New York Section of the American Chemical Society, White Plains, NY, March. 14, 2008.
23. "Structural DNA Nanotechnology: Information Guided Self-assembly", Division of Chemistry and Chemical Engineering, California Institute of Technology, Pasadena, CA, March. 12, 2008.
24. "Structural DNA Nanotechnology: Information Guided Self-assembly", Department of Chemistry, U. of Central Florida, Orlando, FL, Oct. 12, 2007.
25. "DNA based self-assembly of nanostructures", symposium MM: Biomolecular and Biologically-Inspired Interfaces and Assemblies, Fall 2007 Materials Research Society National Meeting, Boston, MA, Nov 27-Dec. 1, 2007.
26. "DNA based self-assembly of nanostructures", symposium on Advances in Bio-based Nanostructures and Nanomaterials, 234th ACS National Meeting, Boston, MA, Aug. 19-23, 2007.
27. "DNA based self-assembly of nanostructures", Mini-symposium on DNA based Nanotechnology University of Aarhus, Aarhus, Denmark, Aug. 17, 2007.
28. "DNA based self-assembly of nanostructures", The Second Advanced Materials Workshop, Dalian, China, June 23-24, 2007.
29. "DNA based self-assembly of nanostructures", Albany 2007: The 15th Conversation, Albany, New York, June 21, 2007.
30. "DNA based self-assembly of nanostructures", NSF Center for Hierarchical Manufacturing, U. of Massachusetts, Amherst, MA, May 17, 2007.

Awards and Honors:

Alfred P. Sloan Research Fellowship, 2008
ASU Promotion and Tenure Faculty Exemplar 2008